All Printed Flexible Piezoelectric Pressure Sensor with Interdigitated Electrodes

Karem Lozano Montero, Mika-Matti Laurila, Matti Mäntysalo
Faculty of Information and Communication Sciences
Tampere University
Korkeakoulunkatu 3
FI-33720, Tampere, Finland
karem.lozanomontero@tuni.fi

Abstract—**Owing to their cost-effective fabrication, skin-conformability, and charge generation, printed flexible piezoelectric pressure sensors based on poly(vinylidenefluoride-co-trifluoroethylene) P(VDF-TrFE) have high potential to be used in affordable, unobtrusive and energy-autonomous systems for various healthcare and robotics applications. This study presents a simple two printing step fabrication process for a thin (overall thickness of ~11 μm) flexible piezoelectric sensor based on an interdigitated electrode (IDE) structure. Inkjet printing is used to fabricate a poly(3,4-ethylenedioxythiophene): poly(styrene sulfonate) (PEDOT:PSS) IDE structure with an electrode gap width of 67.9 ± 9.4 μm and an electrode width of 137.8 ± 17.5 μm on a Parylene-C substrate. This is followed by bar coating a layer of piezoelectric polymer (P(VDF-TrFE)) of 9.6 ± 0.9 μm thick. The optimal electric field for poling the piezoelectric material is 50 V/μm which results in a remanent polarization of 5.2 ± 1.0 μC/cm². The piezoelectric sensitivity was measured in normal mode obtaining a result of 3.9 ± 0.5 pC/N. In conclusion, this study demonstrates the potential of additive fabrication technologies to develop low-cost and conformal piezoelectric pressure sensors.**

Keywords— Printed electronics, interdigitated electrodes, pressure sensor, e-skin, P(VDF-TrFE).

I. INTRODUCTION

Recently, flexible piezoelectric pressure sensors have drawn wide interest in the research community. There is a broad range of applications where these sensors can be used such as flexible electronic skin (E-skin) (e.g. soft robotics, prosthetics), healthcare monitoring (e.g. pulse-wave measurements), wearable devices (e.g. smart wristband), and industrial applications (e.g. structural health monitoring) [1][2]. Among these applications, these types of sensors are being highly developed for biomedical applications. The trend in this research field is to fabricate very thin sensors that can be attached directly to the human skin without the use of adhesives[3]. This characteristic makes such sensors skin-conformable and unobtrusive for the user thereby eliminating some drawbacks of thick and rigid sensors. This feature also improves the quality of the acquired signals from the skin through a better mechanical coupling. Furthermore, ultra-thin piezoelectric sensors are more sensitive to mechanical deformations [4]. Nevertheless, their reusability is limited because of their minimal thickness which leads them to be very fragile. Thus, cost-effective fabrication methods are required to minimize fabrication costs and material consumption [5]. Transfer processes and photolithography have been previously used for the fabrication of ultra-thin and high sensitivity piezoelectric sensors, but they are characterized because of their low throughput, high material consumption, and biocompatibility issues. In contrast, solution-based printing technologies can considerably decrease production costs, material waste, and simplify the fabrication process [6].

Furthermore, biocompatibility is a key property when sensors interface with biological tissues. There is a tendency of developing piezoelectric sensors based on organic piezoelectric materials such as polymers. These materials are being highly investigated because of their high mechanical stability and compatibility with solution-based printing technologies [7]. For instance, poly(vinylidene fluoride) (PVDF) based copolymers are a promising class of piezoelectric materials that can be used in medical applications because of being biocompatible and environment-friendly [8][9]. Printed piezoelectric pressure sensors based on the piezoelectric polymer poly(vinylidenefluoride-co-trifluoroethylene) (P(VDF-TrFE)) have been demonstrated [8][10][11]. Using polymers and printed electronics technologies eliminate biocompatibility issues and decrease production costs. Nonetheless, the sensors usually are fabricated on a relatively thick substrate, and an adhesive patch must be used to attach the sensors to the skin. Therefore, minimizing the overall thickness can improve the conformability of the sensors.

Additionally, the sensor configuration can have an impact on its performance. The most common structures used in piezoelectric sensors are metal-insulator(piezoelectric)-metal (MIM) and interdigitated electrode (IDE) structures. The generated output voltage of IDE-based sensors is higher compared to MIM-based sensors with similar dimensions [12]. In IDE-based piezoelectric sensors, the term "interdigitated" is referring to a finger-like pattern repeated periodically. A thin layer of conductive material is distributed on the substrate to build two electrodes with an interdigitated approach, and the active material is deposited on top of the electrodes. Using the IDE structure reduces the number of processing steps which eliminates possible challenges related to annealing conditions and pin-hole formation when fabricating MIM-based sensors. Furthermore, IDE-based sensors exhibit a smaller capacitance compared to MIM-based sensors which should lead to a higher output voltage. Therefore, owing to the characteristics of IDE-based sensors (i.e. higher output voltage and fewer fabrication steps), developing piezoelectric pressure sensors based on this configuration can be advantageous.

In this research, we investigate the design and fabrication of a flexible piezoelectric pressure sensor based on an IDE structure using printed electronics technologies. The sensor is built onto a highly flexible Parylene C substrate. Inkjet printing is used to fabricate the IDE structure using poly(3,4-ethylenedioxythiophene):poly(styrene sulfonate) (PEDOT:PSS) ink. Then, the piezoelectric layer is coated on top of the electrodes using P(VDF-TrFE) ink. Moreover, the piezoelectric properties of the samples are analyzed. The piezoelectric sensitivity in normal mode is also measured. The purpose of the characterization measurements is to validate the suitability of the presented methodology for the

fabrication of piezoelectric pressure sensors with IDE structure.

II. EXPERIMENTS

A. IDE sensor fabrication

The fabrication process of the sensors developed in this research is depicted in Fig. 1. Glass wafers were used as carriers for sensor fabrication. First, glass wafers were cleaned and sonicated in deionized (DI) water and soap, DI water, acetone, and isopropanol for 20 minutes each. These carriers were spin-coated with polytetrafluoroethylene (PTFE) to form a release layer. Then, a Parylene-C (GALXYL C Galentis) layer, of approximately 1 µm thick, was deposited on the glass carrier using chemical vapor deposition (LabTop 3000, Para Tech Coating). Samples were treated in a UV/O$_3$ surface cleaner (PSD-UV, Novascan) for 15 minutes before printing. An IDE structure was inkjet-printed (DMP-2801, Fujifilm Dimatix) using PEDOT:PSS ink (Clevios P Jet 700, Heraeus) with the following printing parameters: 40 µm drop spacing, cartridge temperature of 38 °C, and stage at room temperature. The printed sample was annealed in a convection oven at 130 °C for 15 minutes. P(VDF-TrFE) ink (Ink P, Piezotech Arkema Group) was deposited on top of the electrodes using an automatic bar coater (Motorized Film Applicator CX4, MTV Messtechnik). Subsequently, the samples were annealed at 135 °C for 1 hour in a convection oven. This was followed by the poling process which is required to activate the piezoelectric properties of the P(VDF-TrFE) layer. This was done using the ferroelectric characterization tool (aixACCT TF2000, aixACCT Systems GmbH) coupled with a high-voltage amplifier (610C, TREK) while doing the polarization-electric (PE) field hysteresis loops measurements (see section II C).
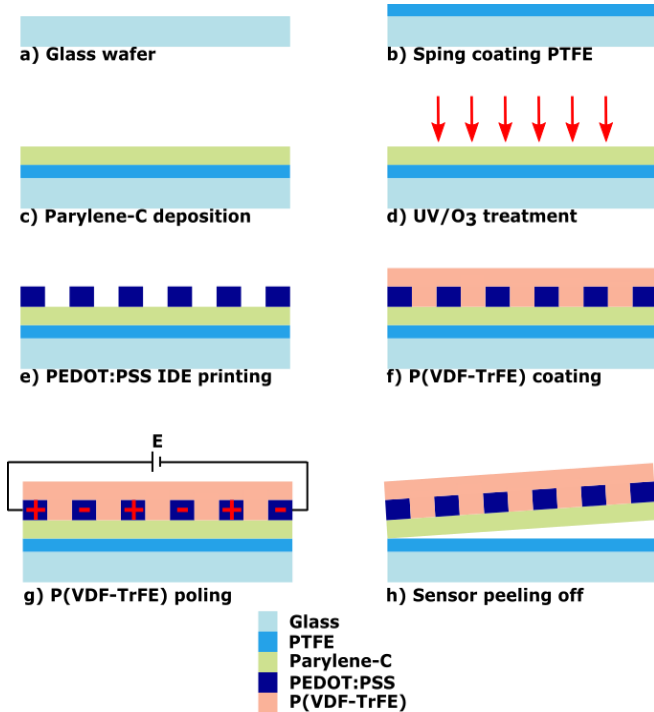

Fig. 1. IDE sensor fabrication process. E is the applied electric field calculated based on Eq. (1).

B. Characterization of sensor dimensions

The gap width between the electrode fingers and the electrode fingers width were measured using an optical microscope (BX60M, Olympus). Multiple measurements were taken from three positions of the IDE structure. The thickness of the P(VDF-TrFE) layer was measured using a stylus profilometer (Dektak XT, Bruker).

C. Piezoelectric and electrical characterization.

The polarization-electric field (PE) hysteresis loops were measured using a ferroelectric tester (aixACCT TF2000, aixACCT Systems GmbH) connected to a 10 kV voltage amplifier (610C, TREK). The frequency of the measurements was 2.5 Hz. The PE loop was measured at 50, 60, 70, and 80 V/µm in steps of 10 V/µm. The applied electric field is described by Eq. (1) where V is the applied voltage and G is the gap width between electrode fingers (see Fig. 3).

$$E = \frac{V}{G} \qquad (1)$$

The piezoelectric sensitivity of the samples was measured using a piezometer (PiezoMeter PM300, Piezotest). The measurement setup is depicted in Fig. 2. A static force of 10 N was used to press the sensor between the probes. Circular flat probes with a diameter of 10 mm were used to activate multiple electrode finger pairs. Then, a dynamic force of 0.25 N with a frequency of 110 Hz was applied to the samples. The sensitivity was measured from five positions. The average value of the measurements was calculated to determine the piezoelectric sensitivity of the sensors in normal mode.
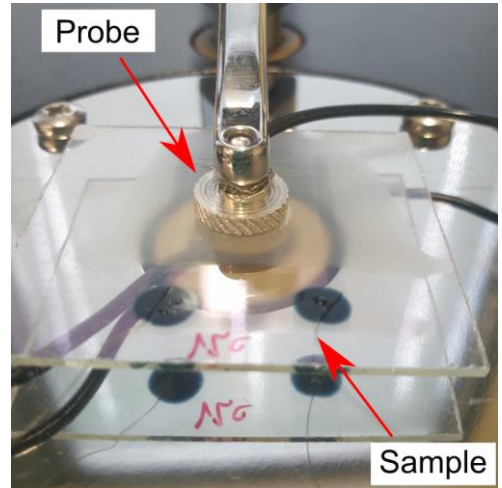

Fig. 2. Piezoelectric sensitivity measurement setup.

III. RESULTS AND DISCUSSION

A. Sensor dimensions

The IDE design is depicted in Fig. 3, and the resulting IDE sensor is shown in Fig. 4a. The designed gap width (G) and electrode finger width (W) were 40 µm and 140 µm, respectively, and the designed overlapping length (L) of the electrodes was 14.6 mm. However, the true dimensions of the IDE are affected by the chosen print parameters and substrate wettability. For example, the uniformity of inkjet printed lines is influenced by the drop spacing and the time delay between droplet deposition. In general, five morphologies can be observed in inkjet printed lines [13]. When the drop spacing is larger than the drop diameter, individual drops are formed. Then, when the drop spacing is decreased drops start to merge forming scalloped lines. Uniform lines are created by further decreasing the drop spacing. However, if the drop spacing is

very small, bulged lines are formed. Moreover, if the evaporation of a droplet occurs faster than the time delay between the deposition of the subsequent droplet, individual drops will have time to dry and this will result in a stacked coin pattern. It is therefore important to optimize the substrate wettability and print parameters to achieve uniform lines. In this study, the optimized wetting conditions were achieved by treating the Parylene-C substrate in a UV/O$_3$ chamber for 15 minutes. The resulting IDE fingers are depicted in Fig. 4c.
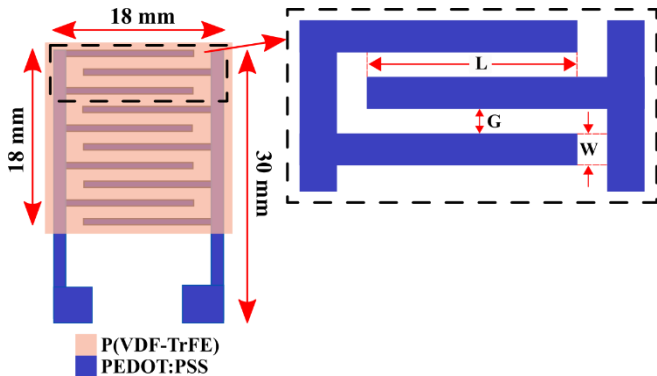

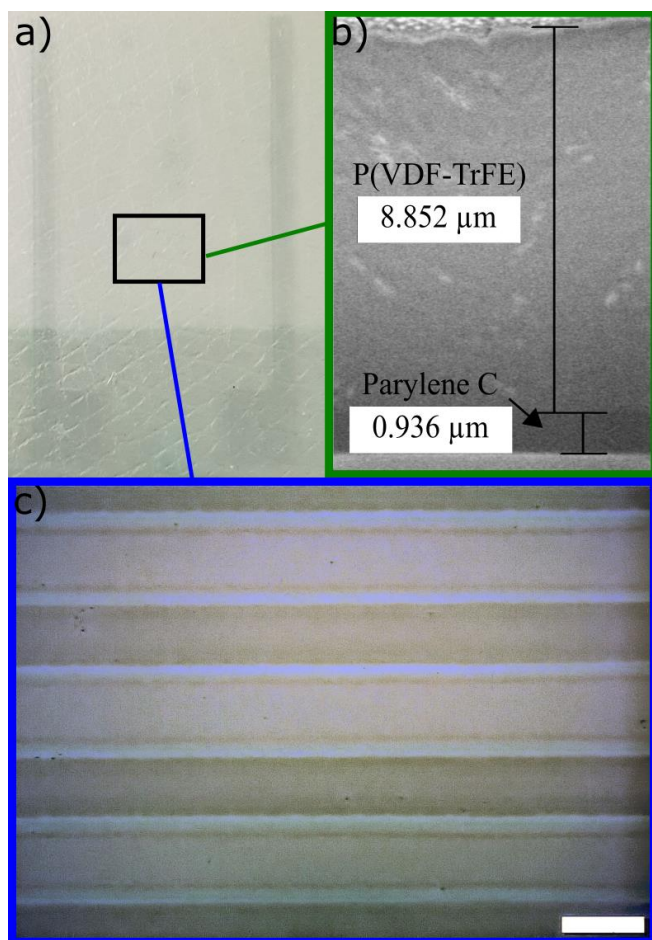Fig. 3. The designed dimensions of the IDE sensor.

Fig. 4. IDE sensor. a) IDE sensor on glass carrier. b) SEM image of the FIB cross-section of the IDE sensor (scale bar 1 µm). c) Optical microscope image of the IDE fingers (scale bar 100 µm).

The uniformity of the electrode fingers was analyzed by measuring the electrode width (W) and gap size (G). The mean electrode width was 137.8 ± 17.5 µm, and the mean gap width was 67.9 ± 9.4 µm. The measured dimensions of the

printed pattern do not correspond to the designed dimensions because the width of a printed line depends on the overlap of the drops during the printing process. Furthermore, this is affected by the droplet diameter and how the ink is spread on the substrate. Moreover, the variation of the gap width has an impact on the uniformity of the applied electric field during the PE-loop measurements (see Eq. (1)) and this may lead to inhomogeneous polarization of the piezoelectric material. Additionally, the applied electric field may be extremely high in some regions, which may lead to a dielectric breakdown of the piezoelectric material. The high instantaneous current will then cause the electrode to burn thereby creating an open circuit and resulting in a non-working electrode. In addition, the capacitance of the IDE sensors is determined by the gap width and the number of electrodes[14]. Consequently, if the number of working electrode pairs decreases due to dielectric breakdown, then the capacitance of the device will also be affected by these variations.

Although the uniformity of the piezoelectric layer of IDE-based sensors is not as critical as in MIM-based sensors, a high disparity of the thickness across the piezoelectric layer could lead to performance variations. It is therefore important to also optimize the uniformity of the piezoelectric layer thickness. For this purpose, the dry thickness of the bar coated P(VDF-TrFE) layer was characterized for a set of three different wet thicknesses: 60 µm, 100 µm, and 140 µm. Three samples were fabricated for each case and their thicknesses were measured from three positions. To characterize the uniformity of the printed layers, the percent relative range was then calculated by dividing the range of the measured values by their mean value. The P(VDF-TrFE) layers fabricated using a wet thickness of 140 µm showed the lowest percent relative change of 25%. Therefore, this wet thickness was chosen to be used for the final samples. The mean thickness of the final samples was 9.6 ± 0.9 µm which shows that the printed P(VDF-TrFE) layer was very uniform. Taking into account the ~1 µm thick Parylene-C substrate, the overall thickness of the sensors should be then 10-11 µm. This was verified by performing a FIB cross-section on one sample and characterizing it with SEM (see Fig. 4b). As demonstrated in Fig. 5, the minimal sensor thickness results in high skin conformability and unobtrusiveness.

Fig. 5. IDE sensor attached to the skin.

B. PE-loop measurements

PVDF-based polymers are characterized by exhibiting at least four types of crystalline phases (i.e. α, β, γ, and δ structures). Among these, the β-phase is the crystalline phase

that shows the strongest piezoelectricity. P(VDF-TrFE) copolymer readily crystallizes into the β-phase. However, because the electric dipoles of the domains are randomly oriented in pristine P(VDF-TrFE), the net polarization across the material is zero. Electrical poling of the material is therefore required to align the dipoles and to enhance its piezoelectric properties [15].

The polarization electric field (PE) hysteresis loop describes the variation of material polarization (P) depending on the applied electric field (E). The electric field is simply the voltage applied over the material thickness, while the polarization is determined by the generated charges (Q) and the effective electrode area (A) where the charges are collected, i.e. $P = Q/A$ [16]. Therefore, to calculate the polarization value from the PE-loops, it was first necessary to determine the effective electrode area of the IDE structure. Fig. 6 illustrates the transition from a metal-insulator-metal type sensor (i.e. MIM) to our IDE type sensor. For MIM structures, the effective electrode area A is simply the overlapping area of the electrodes. Thus, for our IDE type structure, the effective electrode area must be the overlapping area of the parallel finger electrodes multiplied by the number of electrode pairs:

$$A = \frac{(L \cdot W)}{2}(N - 1) \qquad (2)$$

where N represents the number of electrode fingers, L is the overlapping length between two consecutive electrode fingers, and W is the mean electrode width (see Fig. 3). The effective area was calculated separately for each sample based on their dimensions.
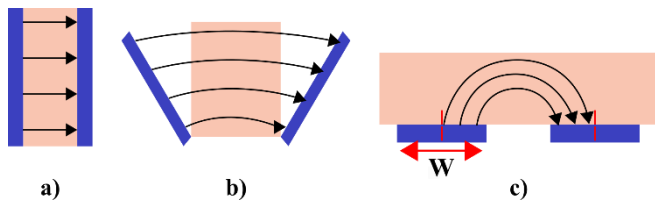

Fig. 6. The transition from a MIM structure to IDE structure. The arrows represent the direction of the electric field. a) MIM structure, b) the electrodes are opened to form a c) planar structure.

Generally, the piezoelectric materials are characterized by measuring parameters such as remanent polarization (P_r) and coercive field (E_c), whereas piezoelectric sensors are best characterized by measuring their piezoelectric sensitivity (i.e. the amount of charge generated by unit of force/pressure). The remanent polarization and coercive field of a piezoelectric material can be determined from the PE hysteresis loop. When an increasing electric field is applied to a non-poled piezoelectric material, the net polarization across it increases as the dipoles in the material domains become increasingly aligned. This takes place at a material dependent threshold electric field value (i.e. coercive field E_c). However, when the electric field is subsequently decreased, the dipoles remain aligned such that even when the electric field is reduced to zero, the material remains polarized (i.e. remanent polarization P_r). In short, the remanent polarization is the polarization value when the applied electric field is zero, and the coercive field indicates the electric field that is required to switch the direction of the polarization. These points are depicted in Fig. 7a which shows the progression of the PE hysteresis loop for a typical IDE sample.

The variation of the remanent polarization in relation to the applied electric field is illustrated in Fig. 7b for eight samples. The highest measured P_r value was 6.7 μC/cm^2 which is similar to the P(VDF-TrFE) literature value of 6 to 7 μC/cm^2 [18]. The mean remanent polarization of the samples for an electric field of 50 V/μm was 5.2 ± 1.0 μC/cm^2, and the mean coercive field was 35.4 ± 3.2 V/μm. Table I summarizes the P_r and E_c mean values of all samples for each applied electric field. As can be seen, the mean remanent polarization seems to decrease when increasing the electric field. The likely cause for this is the dielectric breakdown that occurs in some of the samples. As can be seen in Fig. 7b, the remanent polarization of samples S3, S5, S6, and S8 shows a decrease of over 35% between 50 V/μm and 80 V/μm. In contrast, the remanent polarization of samples S1, S2, S4, and S7 remains almost the same, or even increases slightly. Therefore, the samples were divided into two groups: samples with low P_r (termed "dielectric breakdown") and samples with high P_r (termed "no dielectric breakdown"). The mean remanent polarization of the samples divided by groups are listed in Table I. The decrease of the remanent polarization implies that the amount of collected charges is lower. This occurs because the number of working electrode finger pairs decreases which implies that the dielectric breakdown generates open circuits in the electrodes instead of shorts as in MIM-based sensors. This could be beneficial since some areas of the sensor remain active despite the P(VDF-TrFE) dielectric breakdown. However, our results also suggest that a relatively high remanent polarization (5.2 ± 1.0 μC/cm^2) can be achieved already at an electric field value of 50 V/μm, which also minimizes the probability of dielectric breakdown. In summary, these results suggest that the optimal electric field for poling process is 50 V/μm.
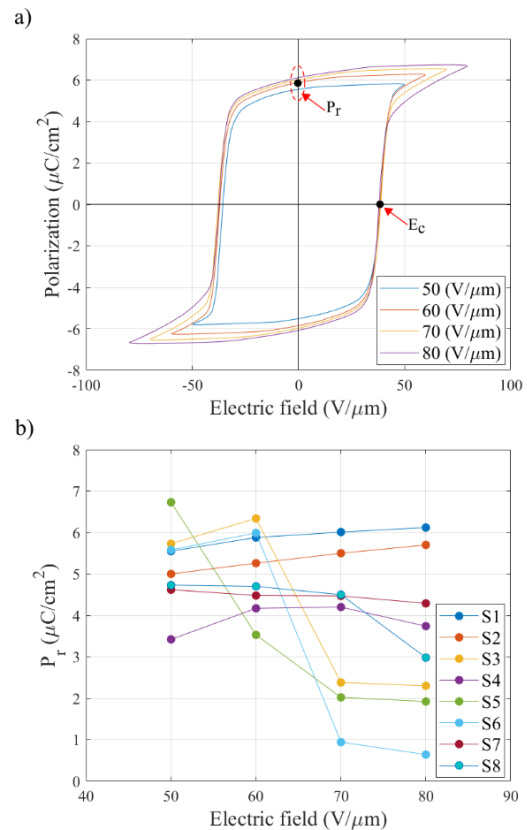
a)

b)

Fig. 7. a) Progression of PE-loop for sample S1. b) Remanent polarization variation for a set of eight samples.

TABLE I.   REMANENT POLARIZATION AND COERCIVE FIELD OF ALL THE SAMPLES.

Electric Field (V/µm)	All samples		No Dielectric breakdown	Dielectric breakdown
	P_r (µC/cm²)	E_c (V/µm)	P_r (µC/cm²)	P_r (µC/cm²)
50	5.2 ± 1.0	35.4 ± 3.2	4.6 ± 0.8	5.7 ± 0.7
60	5.0 ± 1.0	37.8 ± 3.7	4.9 ± 0.7	5.1 ± 1.1
70	3.8 ± 1.8	40.3 ± 3.1	5.0 ± 0.7	2.5 ± 1.3
80	3.5 ± 1.9	46.5 ± 8.3	5.0 ± 1.0	2.0 ± 0.9

Then, the coefficient of variation (CV) of the electrode width and gap width was analyzed for each sample group (i.e. "dielectric breakdown" and "no dielectric breakdown"). The results are summarized in Table II. The measurements indicate, that for the samples with a dielectric breakdown, the CV of the electrode width was 5 percentage points higher than in the case where no dielectric breakdown occurred. Moreover, the measured gap width values of the samples with dielectric breakdown also showed a CV of 3 percentage points higher. These results highlight the importance of electrode uniformity in the fabrication of the IDE based piezoelectric sensors.

TABLE II.   COEFFICIENT OF VARIATION OF ELECTRODES WIDTH AND GAP SIZE: NO DIELECTRIC BREAKDOWN (S1, S2, S4, AND S7) AND DIELECTRIC BREAKDOWN (S3, S5, S6, AND S8)

Parameter	No Dielectric breakdown	Dielectric breakdown
W	7 %	12 %
G	18 %	21 %

C. Piezoelectric Sensitivity

The piezoelectric sensors can be used to measure the dynamic pressure because the generated charges are proportional to the mechanical deformation produced by the applied pressure. The piezoelectric sensitivity of the sensor (i.e. the amount of charge per unit force or pressure) can be used to describe the performance of such sensors. To compare the performance of the IDE type sensors to the MIM type sensors fabricated in our previous study [19], the piezoelectric sensitivity of the samples with no dielectric breakdown was measured in normal mode (i.e. force applied perpendicular to the substrate plane). The normal mode sensitivity measurement corresponds to the $d_{33.f}$ piezoelectric coefficient measurement performed in our previous study for the MIM type sensor.

The measurements were done in five points of the IDE samples. Fig. 8 shows a boxplot of the normal mode piezoelectric sensitivity for four samples, and the measurements of a non-poled sample are also represented. The results show that the mean sensitivity of the samples is 3.9 ± 0.5 pC/N. Moreover, the mean CV of the sensitivity measurements was 13%, which indicates that the measured sensitivity varied depending on the area of the sensor where the force was applied. This occurs probably because of the non-uniform poling of the P(VDF-TrFE) layer resulting from the variation of the sensor dimensions (as explained in Section III B). Compared to the previously fabricated MIM type sensors, the normal mode sensitivity was 85% lower. However, the output voltage of the IDE-based sensors should be higher because of their significantly smaller capacitance

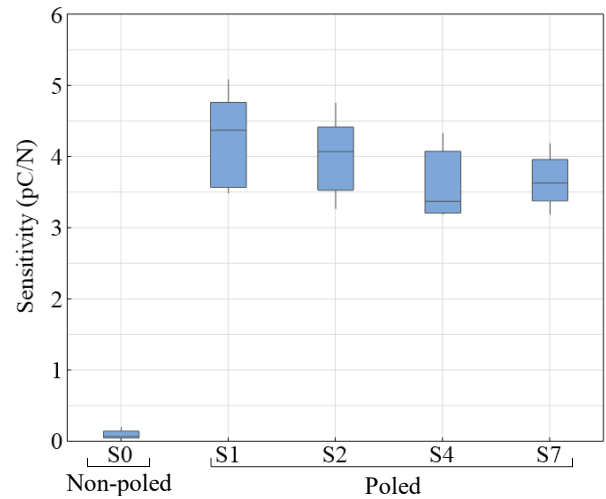of 54.4 pF compared to the capacitance of the MIM-based sensors of 1.6 nF.

Fig. 8.   Boxplot of piezoelectric sensitivity in normal mode for four samples.

IV. CONCLUSIONS

In this study, we have demonstrated a simple two printing step fabrication of a flexible piezoelectric pressure sensor with interdigitated electrodes using printed electronics fabrication tools. The overall thickness of the sensor was approximately 11 µm. The obtained minimal thickness allows the conformability of the sensor onto the skin without the use of adhesives. Furthermore, the piezoelectric characterization of the sensor indicates that it was possible to polarize the P(VDF-TrFE) layer following the methodology developed in this study. However, owing to the non-uniformities of the printed IDE structure (gap width of 67.9 ± 9.4 µm and electrode finger width of 137.8 ± 17.5 µm), the polarization of the piezoelectric material was inhomogeneous across the electrodes and therefore in some cases, the remanent polarization of the samples was lower compared to the literature value. In addition, the P(VDF-TrFE) dielectric breakdown had an impact on the sensor performance at high electric fields. Nevertheless, a mean remanent polarization of 5.2 ± 1.0 µC/cm² was achieved already at an electric field of 50 V/µm. Additionally, the piezoelectric sensitivity in normal mode was measured to be 3.9 ± 0.5 pC/N. This result shows the potential use of this sensor in applications where mechanical deformation has to be detected (e.g. non-invasive arterial pulse-wave measurement). Nonetheless, the optimization of the fabrication process has to be done to improve the piezoelectric properties of the sensor. In conclusion, the additive fabrication methodology used in this study could be beneficial to develop low-cost sensors that may be used in wearable electronics applications.

References

[1] Y. Zang, F. Zhang, C. A. Di, and D. Zhu, "Advances of flexible pressure sensors toward artificial intelligence and health care applications," Mater. Horizons, vol. 2, no. 2, pp. 140–156, 2015.

[2] F. Xu et al., "Recent developments for flexible pressure sensors: A review," Micromachines, vol. 9, no. 11, p. 580, Nov. 2018.

[3] F. A. Viola, A. Spanu, P. C. Ricci, A. Bonfiglio, and P. Cosseddu, "Ultrathin, flexible and multimodal tactile sensors based on organic field-effect transistors," Sci. Rep., vol. 8, no. 1, Dec. 2018.

[4] Y. Wang et al., "Low-cost, μm-thick, tape-free electronic tattoo sensors with minimized motion and sweat artifacts," npj Flex. Electron., vol. 2, no. 1, p. 6, 2018.

[5] M. M. Laurila et al., "A fully printed ultra-thin charge amplifier for on-skin biosignal measurements," IEEE J. Electron Devices Soc., vol. 7, pp. 566–574, 2019.

[6] J. C. Yang, J. Mun, S. Y. Kwon, S. Park, Z. Bao, and S. Park, "Electronic Skin: Recent Progress and Future Prospects for Skin-Attachable Devices for Health Monitoring, Robotics, and Prosthetics," Adv. Mater., vol. 0, no. 0, p. 1904765, Sep. 2019.

[7] X. Wang, Z. Liu, and T. Zhang, "Flexible Sensing Electronics for Wearable/Attachable Health Monitoring," Small, vol. 13, no. 25, p. 1602790, Jul. 2017.

[8] S. H. Park, H. B. Lee, S. M. Yeon, J. Park, and N. K. Lee, "Flexible and Stretchable Piezoelectric Sensor with Thickness-Tunable Configuration of Electrospun Nanofiber Mat and Elastomeric Substrates," ACS Appl. Mater. Interfaces, vol. 8, no. 37, pp. 24773–24781, Sep. 2016.

[9] M. T. Chorsi et al., "Piezoelectric Biomaterials for Sensors and Actuators," Adv. Mater., vol. 31, no. 1, p. 1802084, Jan. 2019.

[10] T. Sekine et al., "Fully Printed Wearable Vital Sensor for Human Pulse Rate Monitoring using Ferroelectric Polymer," Sci. Rep., vol. 8, no. 1, p. 4442, 2018.

[11] D. Thuau, K. Kallitsis, F. D. Dos Santos, and G. Hadziioannou, "All inkjet-printed piezoelectric electronic devices: Energy generators, sensors and actuators," J. Mater. Chem. C, vol. 5, no. 38, pp. 9963–9966, 2017.

[12] K. Il Park et al., "Highly-efficient, flexible piezoelectric PZT thin film nanogenerator on plastic substrates," Adv. Mater., vol. 26, no. 16, pp. 2514–2520, Apr. 2014.

[13] D. Soltman and V. Subramanian, "Inkjet-printed line morphologies and temperature control of the coffee ring effect," Langmuir, vol. 24, no. 5, pp. 2224–2231, Mar. 2008.

[14] J. C. Park, J. Y. Park, and Y. P. Lee, "Modeling and characterization of piezoelectric d33-Mode MEMS energy harvester," J. Microelectromechanical Syst., vol. 19, no. 5, pp. 1215–1222, Nov. 2010.

[15] J.-H. Bae and S.-H. Chang, "Characterization of an electroactive polymer (PVDF-TrFE) film-type sensor for health monitoring of composite structures," Compos. Struct., vol. 131, pp. 1090–1098, 2015.

[16] W. J. Hu et al., "Universal Ferroelectric Switching Dynamics of Vinylidene Fluoride-trifluoroethylene Copolymer Films," Sci. Rep., vol. 4, no. 1, p. 4772, 2014.

[17] K. El-Hami, A. Ribbe, S. Isoda, and K. Matsushige, "Structural analysis of the P(VDF/TrFE) copolymer film," Chem. Eng. Sci., vol. 58, no. 2, pp. 397–400, 2003.

[18] PiezoTech Arkema, "TDS PIEZOTECH® FC INK P For Printed Organic Electronics, Smart Textiles and Plastronics." 2018.

[19] M. M. Laurila et al., "Evaluation of printed P(VDF-TrFE) pressure sensor signal quality in arterial pulse wave measurement," IEEE Sens. J., p. 1, 2019.